Synchrotron radiation analysis of structure and magnetism of grain boundary phase in Nd-Fe-B sintered magnet

T. Nakamura, A. Yasui, W. Ueno, N. Tsuji, T. Ohkubo[*], H. Iwai[*], T. Akiya[*], Y. Kotani, T. Fukagawa[**], T. Nishiuchi[**], Y. Gohda[***], K. Hono[*], and S. Hirosawa[*]
(JASRI/SPring8, [*]NIMS, [**]Hitachi Metals Ltd., [***]Univ. of Tokyo)

A high performance Nd-Fe-B permanent magnet has become an indispensable material for electric products, hybrid vehicles, and power generators, which are key technologies for energy sustainability. Associating with problem on the critical materials, improvement in coercivity without reduction of magnetization is intensely required in Dy-free type Nd-Fe-B magnets. Since it has been known that microstructure is essential for permanent magnets in order to increase the coercivity, the microstructure control may, therefore, bring a solution to developing the high performance Dy-free Nd-Fe-B sintered magnet. In a micro-magnetic point of view, a thin-film-like grain boundary (GB) phase existing between neighboring $Nd_2Fe_{14}B$ grains is preferred to be paramagnetic so as to prevent reversed magnetic domains from expanding into neighboring grains. Although the GB phase had been believed to be paramagnetic for a long time, the recent study using a three dimensional laser atom probe technique by Sepehri-Amin *et al*. showed convincing results indicating that the amorphous GB phase could be ferromagnetic [1]. Further studies on magnetism of the GB phase, however, are needed to uncover the origin of the coercivity.

In the present work, we have measured X-ray magnetic circular dichroism (XMCD) spectra in a $Nd_{14.0}Fe_{79.7}B_{6.2}Cu_{0.1}$ sintered magnet using synchrotron soft X-rays at BL25SU of SPring-8 in order to clarify the magnetic state of the GB phase. Since the Nd-Fe-B sintered magnets have a grain-boundary fracturing character, magnetism of the GB is directly investigated by the surface-sensitive XMCD measurement using a total electron yield (TEY) method [2]. The XMCD of the Fe $L_{2,3}$-edges was measured on the fractured surface which was covered with the GB phase. Applying the magneto optical sum rule [3-5], the apparent Fe magnetic moment was obtained as 1.66 μ_B from the XMCD spectra measured at 30 °C. Since the recorded XMCD signal was composed of those coming from the GB phase and the under-layered $Nd_2Fe_{14}B$ main phase, the magnetic moment of 1.66 μ_B was deconvoluted into each contribution on assumption of the probing depth of the TEY (λ_e=1.2 nm) at the Fe $L_{2,3}$-edges [2] and a thickness of the GB phase (t_B=3 nm) [1]. As the result of the deconvolution analysis, the Fe magnetic moment of the GB phase was estimated as 1.4 μ_B. This value is of about 60 % compared to that of $Nd_2Fe_{14}B$ and implies that the GB phase is ferromagnetic. Moreover, the temperature dependence of Fe magnetic moment in Fig. 1, which was obtained from the XMCD spectra, indicated that the Curie temperature of the GB phase was lower than that of the main phase, $Nd_2Fe_{14}B$. The present result, therefore, implies that the coercivity will possibly be improved by forming the GB phase which has the Curie point being lower than the operating temperature.

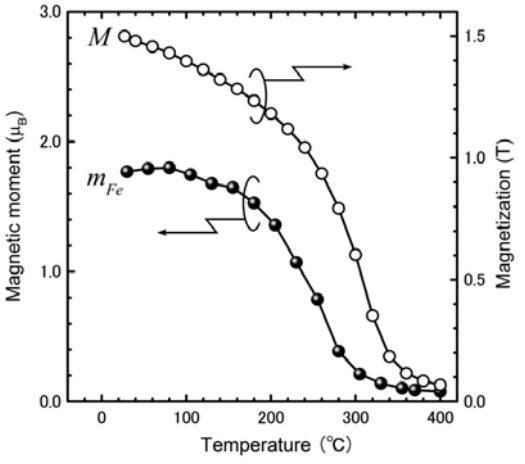

Fig. 1 Temperature dependence of Fe magnetic moments (m_{Fe}) obtained by sum rule analysis of XMCD spectra at the Fe $L_{2,3}$-edges and a magnetization (M). Both XMCD and magnetization were measured under 1.9 T.

It was reported that the thin-film-like GB phase grows by post-sintered annealing process [1]. The materials to form the GB phase could be supplied from somewhere like the Nd-rich phase at the triple junction during the annealing process. In order to elucidate the metallurgical phenomena with respect to the constitutional phases, we have investigated the crystal phases in the $Nd_{14.0}Fe_{79.7}B_{6.2}Cu_{0.1}$ sintered magnet by X-ray diffraction (XRD) experiment up to 1000 °C. High temperature *in-situ* XRD measurements were performed at BL02B2 of SPring-8. In

previous studies by means of transmission electron microscopy (TEM) [6, 7], it has been reported that the Nd-rich phase is a mixture of Nd ($P6_3/mmc$), Nd_2O_3 ($P6_3/mmc$), NdO_x ($Fm\bar{3}m$), and small amounts of other compounds, where symbols in parentheses denote the space groups of crystallography. Among them, the Nd-metal phase is expected to relate to the formation of the GB phase because the optimum annealing temperature of 540 °C is very close to the eutectic point of 520 °C in the Cu-Nd system. Fig. 2 shows temperature dependence of XRD patterns with labels denoting crystal phases determined by analysis of the XRD patterns. The Nd-metal phase ($P6_3/mmc$) starts melting at 580 °C (XRD pattern at 580 °C is not shown here), and completely melts at 606 °C. The melting point of the metallic Nd phase in the present experiment is higher than that expected from the eutectic point by 60 ~ 80 °C. This difference of the temperature is explained as that the XRD detects the crystalline Nd-metal unused in the eutectic reaction because the Cu concentration (0.1 at%) is too small to consume all of the crystalline Nd phases (>1 at%). Here, the volume fraction of Nd which exists as Nd metal was estimated from the Rietvelt analysis of XRD pattern. On the other hand, a different Nd phase having cubic crystal symmetry ($Fm\bar{3}m$) was also found in the temperature range between 335 ~ 788 °C. Variation in volume fraction of the cubic and hexagonal phases of Nd was invisible at the eutectic point. The Nd2O3 phase remains solid state even at 1000 °C, but shows some phase transitions with respect to crystal symmetries involving $P6_3/mmc$, $Ia\bar{3}$, and $P\bar{3}m1$. Although the mechanism of these phase transitions in the Nd_2O_3 phases is still not clear, the information may be useful in refining the Nd-O phase diagram which is important in elucidation of the microstructural formation mechanism of Nd-Fe-B magnets.

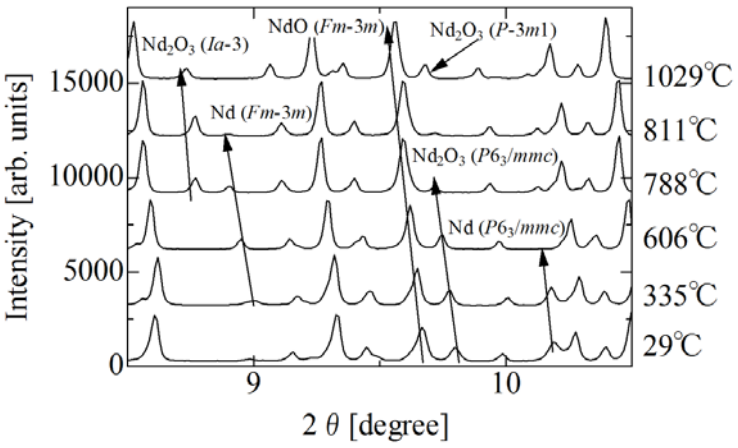

Fig. 2 Temperature dependence of XRD patterns of $Nd_{14.0}Fe_{79.7}B_{6.2}Cu_{0.1}$ sintered magnet. Arrows beside XRD peaks denote trends of shift of peak positions for identified crystalline phases.

Acknowledgements

The authors are grateful to Drs. J. Kim, K. Sugimoto, M. Suzuki, A. Fujiwara, and M. Takata of JASRI, and Dr. H. Sepehri-Amin and T. Abe of NIMS for fruitful discussions. A part of this work is supported by the Elements Strategy Initiative Center for Magnetic Materials under the outsourcing project of MEXT.

References

[1] H. Sepehri-Amin, T. Ohkubo, T. Shima, K. Hono, Acta Mater. **60**, 819 (2012).
[2] B. H. Frazer, B. Gilbert, B. R. Sonderegger, and G. De Stasio, Surf. Sci. **537**, 161 (2003).
[3] B. T. Thole, P. Carra, F. Sette, and G. van der Laan, Phys. Rev. Lett. **68**, 1943 (1992).
[4] P. Carra, B. T. Thole, M. Altarelli, and X. Wang, Phys. Rev. Lett. **70**, 694 (1993).
[5] C. T. Chen, Y. U. Idzerda, H. -J. Lin, N. V. Smith, G. Meigs, E. Chaban, G. H. Ho, E. Pellegrin, and F. Sette, Phys. Rev. Lett. **75**, 152 (1995).
[6] J. Fidler, IEEE Trans. Magn. **21**, 1955 (1985).
[7] Mo W, Zhang L, Liu Q, Shan A, Wu J, Komuro M. Scripta Mater. **59**, 179 (2008).

Effect of grain size reduction of Nd-Fe-B sintered magnet on temperature coefficient of coercivity.

Y. Une, H. Kubo, T. Mizoguchi, T. Iriyama, M. Sagawa, M. Nakamura※, M. Matsuura※, S. Sugimoto※
(Intermetallics Co., Ltd., ※Tohoku Univ.)

1. Introduction

Grain size reduction technique of Nd-Fe-B sintered magnets is well known process to increase a coercivity without substitution of Dy for Nd. We have been developing ultrafine grained Nd-Fe-B sintered magnets using a helium gas jet-mill which can produce smaller particle size of the powder than a conventional nitrogen gas jet-mill[(1)]. Recently, Nakamura *et al*.[(2)] have reported the development of single crystal powders with particle size of under 0.6 μm using a combination of HDDR (hydrogenation-disproportionation-desorption-recombination), hydrogen decrepitation, and the helium gas jet-mill processes. In the present study, we report magnetic properties of ultrafine-grained Nd-Fe-B sintered magnets with grain size of under 1 μm.

2. Experiment

The starting material in this study is the strip-cast (SC) alloy with the nominal composition of $Nd_{27.2}Pr_{4.23}FeB_{0.96}Cu_{0.1}Al_{0.24}Co_{0.95}Fe_{bal.}$(wt%). We prepared 3 kinds of powders with particle sizes of 3, 1 and <1μm. The 3 μm powders and the 1 μm powders were produced by using the nitrogen gas jet-mill and the helium gas jet-mill, respectively. For the <1μm powders, the SC alloys were performed the hydrogen decrepitation followed by HDDR treatment. Subsequently, the HDDR-treated alloys were crushed into ultrafine powders by using the helium gas jet-mill[(2)]. Each powder was filling into a carbon mold and subsequently was aligned with pulse magnetic fields of 5T. Then each powder in the molds was sintered at the optimum temperature in vacuum and annealed at optimum temperature. Magnetic properties were measured by B-H loop tracer from room temperature up to 180℃.

3. Results

Fig.1 shows the variation of the temperature coefficient of the coercivity (β) of the Nd-Fe-B sintered magnet vs a function of temperature interval (T-23℃). The temperature coefficient of the HcJ (β) of the magnets improves from -0.55 to -0.47 %/K between 23 and 180℃ with decreasing the particle size of the starting powders from 3 to under 1 μm.

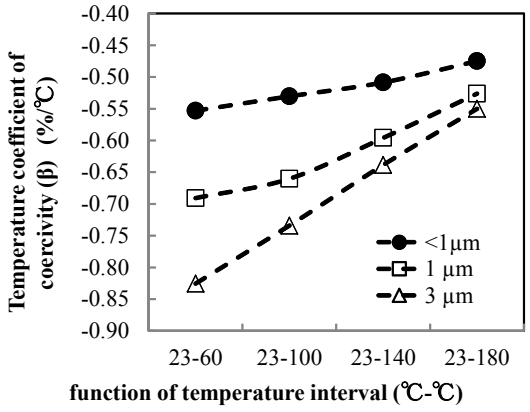

Fig.1 Variation of β of the Nd-Fe-B sintered magnet vs a function of temperature interval.

Reference

1) Y. Une and M. Sagawa, J. Jpan. Inst. Met. **76**, 12(2012) (in Japanese).
2) M. Nakamura *et al*., Appl Phys.Lett. **103**, 022404 (2013).

This study was supported by the "Future Pioneering Projects / Development of magnetic material technology for high-efficiency motors" from the New Energy and Industrial Technology Development Organization (NEDO) of Japan.

Low eutectic temperature alloy diffusion process for hot-deformed Nd-Fe-B magnet

T. Akiya[1], H. Sepheri-Amin[1], J. Liu[1,2], L. Liu[1,2], T. Ohkubo[1], K. Hioki[3], A. Hattori[3], K. Hono[1,2]
[1]Elements Strategy Initiative Center for Magnetic Materials, National Institute for Materials Science
[2]Graduate School of Pure and Applied Science, University of Tsukuba
[3]Daido Steel Co. Ltd.

Nd-Fe-B magnets have been studied for more than thirty years. One of main research issues of Nd-Fe-B magnet is low thermal stability due to its low Curie temperature (T_c ~ 310˚C). To improve the thermal stability, coercivity (H_c) enhancement is a possible way. For example, H_c of 3 T at room temperature (RT) is required for hybrid or pure electric vehicle and wind turbine generator to prevent a thermal demagnetization.

Coercivity of permanent magnet relates to the magnetocrystalline anisotropy field, H_a. The H_a of $Nd_2Fe_{14}B$ phase is about 7 T at RT and the value is theoretical maximum limit of coercivity. However, the coercivity of Nd-Fe-B magnet produced by conventional mass production route is only 1 T without Dy. It is accepted that the surface defects on $Nd_2Fe_{14}B$ particle and inclusions causes the degradation of coercivity, because the nucleation of reversed magnetic domain may occur at these sites. Here, $(Nd,Dy)_2Fe_{14}B$ phase possesses a higher magnetocrystalline anisotropy field than $Nd_2Fe_{14}B$. Therefore, Dy-rich shell structure formed by grain boundary (GB) diffusion process enhances the coercivity effectively with minimum amount of Dy for sintered magnet[1)].

It is empirically known that the coercivity of Nd-Fe-B magnet can be increased by refinement of $Nd_2Fe_{14}B$ crystals without Dy. A Nd-Fe-B sintered magnet with H_c ~ 2 T without Dy had been reported by Intermetallics Co.[2)]. They prepared fine $Nd_2Fe_{14}B$ powder with about 1 μm diameter by He-gas jet-milling technique. However, it is difficult to obtain sub-micron sized powder by jet-milling or any mechanical pulverization technique while preventing oxidation of the powders. Ultrafine $Nd_2Fe_{14}B$ crystal can be obtained by Hydrogenation-Decrepitation-Desorption-Recombination (HDDR) technique or die up setting process of rapidly quenched Nd-Fe-B alloy and then hot-deform processed magnet. These crystal sizes are one order of magnitude smaller than that of sintered magnet, about 300 nm in diameter particle (HDDR) and 300 nm in width and 50 nm in height of platelet shaped grain (hot-deformed), respectively. However, the reported coercivity of ultra-fine grain sized Nd-Fe-B HDDR powders and hot-deformed magnets is only around 1.5 T. This value is lower than expected from a trend of sintered Nd-Fe-B magnet, H_c ~ 2.5 T at 300 nm in diameter[3)].

We have studied the reasons of the low coercivity in three kind of Nd-Fe-B magnets, sintered[4, 5)], HDDR processed powder[6)] and hot deformed Nd-Fe-B magnet[7)]. In any case, the coercivity of Nd-Fe-B magnet relates to structure and chemistry of GB. It have been found that the GB of high coercivity magnet is thicker and contains lower Fe concentration[7)]. Fe-rich GB phase shows ferromagnetic property[5)], therefore, such ferromagnetic GB causes the magnetic coupling between $Nd_2Fe_{14}B$ grains. Thus, magnetic isolation between $Nd_2Fe_{14}B$ grains by nonmagnetic GB layer is critical point to enhance the coercivity.

We demonstrated that the low eutectic alloy diffusion technique is suitable way to modify the structure/chemistry of the grain boundary phase and enhance the coercivity in HDDR powder and hot-deformed magnet. This technique was independently reported by Sepehri-Amin *et al*.[6)] and Mishima *et al*.[8)] in the HDDR processed magnet powders. A low eutectic temperature alloy, such as Nd-Cu, Nd-Al and so on, infiltrates into GB rapidly in HDDR processed powder and hot-deformed magnet and thicker GB layer is formed between $Nd_2Fe_{14}B$ grains without significant grain growth. While, in sintered magnet, Cu diffuses into GB rapidly but the microstructure remains almost unchanged. Thus, the effect of Nd-Cu diffusion process is small in sintered Nd-Fe-B magnet.

Currently, we are focusing on the low eutectic temperature alloy diffusion process for hot deformed magnet. We have observed a coercivity enhancement from 1.5 T to 2.3 T using Nd-Cu eutectic alloy[9)], and 1.6 T to 2.6 T using

$Nd_{60}Dy_{20}Cu_{20}$ near-eutectic alloy[10] for small hot-deformed magnet with 1 mm thickness. While, remanence reduction of about 20 % was also observed due to infiltration of much amount of nonmagnetic material into magnet. After these works, we applied the technique to larger hot-deformed magnet with 5.6 mm thickness, and we confirmed that the infiltration effect occurs almost homogeneously and the coercivity enhancement occurs same as small specimen[11]. In addition, we observed sample expansion to mainly easy direction. The amount of diffusion alloy and volume expansion of magnet was almost comparable. So, we tried an expansion constraint method during diffusion process to prevent the excess diffusion of Nd-Cu phase[12]. As a result, we observed that the diffusion processed hot deformed magnet with constraint possesses higher remanence (M_r = 1.36 T) than simply diffusion processed one (M_r = 1.27 T). One of the reasons can be estimated that the diffusion processed magnet under constraint maintains the higher crystallographic texture than that of as hot-deformed and diffusion processed magnet without applying expansion constraint.

Temperature dependence of H_c and energy density [$(BH)_{max}$] of hot-deformed magnet and the samples that were Nd-Cu diffusion processed with and without an expansion constraint are shown in figure. For comparison, the energy densities of commercial 4% Dy and 8% Dy sintered magnets are also shown[13]. The temperature dependence of coercivity of Nd-Cu diffusion processed magnet is much better than original hot-deformed magnet and 4% Dy sintered magnet. This data suggests that the effect of ultrafine grain $Nd_2Fe_{14}B$ crystals appears by magnetic isolation in high temperature. In addition, the $(BH)_{max}$ of expansion constraint processed hot-deformed magnet is 358 kJ/m^3 at RT and 191 kJ/m^3 at 200 ˚C. This high-temperature property is slightly higher than that of Dy 4% sintered magnet.

We modified the GB of hot-deformed magnet by Nd-Cu diffusion technique. The amount of infiltrated nonmagnetic Nd-Cu into hot-deformed magnet was controlled by expansion constraint diffusion technique. As a result, we could obtain high coercivity as same as 4% Dy containing sintered magnet with high remanence. Obtained magnet possesses higher maximum energy product than 4% Dy containing sintered magnet at 200˚C without Dy. The next step of this work is to realize a magnet with H_c > 0.8 T and $(BH)_{max}$ > 150 kJ/m^3 at 200 ˚C.

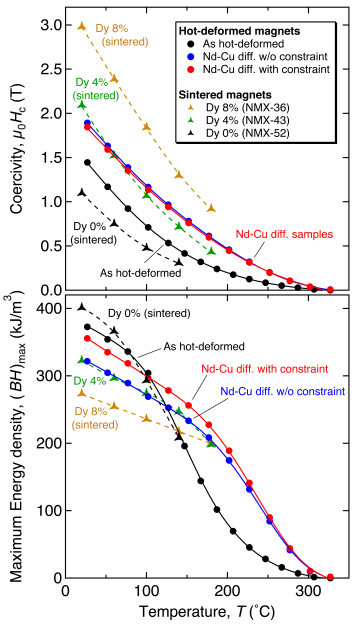

Fig. Temperature dependence of coercivity and maximum energy density.

References

1) H. Nakamura, K. Hirota, M. Shimao, T. Miniwa, M. Honshima, IEEE Trans. Magn. 41 (2005) 3844.
2) Y. Une, M. Sagawa, J. Japan. Inst. Metals, 76 (2012) 12-16.
3) K. Hono, H. Sepehri-Amin, Scripta Mater. 67 (2012) 503.
4) W.F. Li, T. Ohkubo, K. Hono, M. Sagawa, J. Magn. Magn. Mater. 321 (2009) 1100.
5) H. Sepehri-Amin, T. Ohkubo, T. Shima, K. Hono, Acta Mater. 60 (2012) 819.
6) H. Sepehri-Amin, T. Ohkubo, T. Nishiuchi, S. Hirosawa, K. Hono, Scripta Mater. 63 (2010) 1124.
7) J. Liu, H. Sepehri-Amin, T. Ohkubo, K. Hioki, A. Hattori, T Schrefl, K. Hono, Acta Mater. 61 (2013) 5387.
8) C. Mishima, K. Noguchi, M. Yamazaki, H. Mitarai, Y. Honkura. Proceedings of the 21st Workshop on Rare-Earth Permanent Magnets and their Applications, Bled, 29 August 2010, p. 253.
9) H. Sepehri-Amin, J. Liu, T. Ohkubo, K. Hioki, K. Hono, Scripta Mater. 69 (2013) 647.
10) H. Seprhri-Amin, T. Ohkubo, S. Nagashima, M. Yano, T. Shoji, A. Kato, T. Schrefl, K. Hono, Acta Mater. 61 (2013) 6622.
11) T. Akiya, J. Liu, H. Sepehri-Amin, T. Ohkubo, K. Hioki, A. Hattori, K. Hono, J. Appl. Phys. 115 (2014) 17A766.
12) T. Akiya, J. Liu, H. Sepehri-Amin, T. Ohkubo, K. Hioki, A. Hattori, K. Hono, Scripta Mater. 81 (2014) 48.
13) http://www.hitachi-metals.co.jp/products/auto/el/pdf/nmx.pdf

Magnetic domain structure observation of Dy free hot-deformed Nd-Fe-B magnets

Keiko Hioki, Atsushi Hattori, Takahiko Iriyama
(Daido Steel Co., Ltd.)

Nd-Fe-B magnets have a fine microstructure due to their unique fabrication procedure, which gives them 1/10 finer crystal grain size (100~500nm) compared to sintered magnets and produces both better coercivity and reduced Dy content[(1)]. However, the coercivity is not as high as expected from the grain size. To further improve the magnetic properties of this type of magnet, it is important to clarify the reason for the higher coercivity of this magnet. As the first step, we investigated the magnetic domain pattern structure of this magnet in detail.

A hot-deformed Dy-free Nd-Fe-B magnet with the composition of $Nd_{13.5}$-$Co_{3.82}$-$B_{5.64}$-$Ga_{0.57}$-$Fe_{bal.}$ (at.%) was prepared. Its remanence and coercivity were 1.35 T and 1353 kA/m (17.0 kOe), respectively. Observations for this sample were performed from two directions, perpendicular to the c-axis and almost parallel to the c-axis. In this study, the observations of the magnetic domains in the thermally magnetized state and in the magnetization process were performed. These observations were performed using not only Magnetic Force Microscope (MFM) and Atomic Force Microscope (AFM) but also Low Voltage Scanning Electron Microscope (LV-SEM) at the same areas, in order to investigate the relationship between the microstructure and magnetic domain pattern.

Figure 1(a) shows MFM images for the c-plane and (b) shows the illustration of magnetic domain pattern in the same area. Contours of grains observed using LV-SEM are overlaid in the figure. These figures reveal the following: 1. the sample consists of single domain and multi-domain grains, 2. a group of grains form a maze pattern, 3. multi-domain grains exist uniformly throughout the powder, and 4. relatively large grains at the edges of the maze pattern are multi-domain grains. In Fig. 1(c), magnetic domains looking at the plane parallel to the c-axis exhibited the stripe patterns parallel to the c-axis with various widths, some of which are interrupted by the equiaxial grains at powder boundaries. From these observations, the 3D magnetic domain structure of hot-deformed magnet is as portrayed in this figure.

Based on these observations, the magnetic domain structure of hot-deformed Nd-Fe-B magnets will be discussed.

Reference

1)　K. Hioki, A. Hattori, and, T. Iriyama, *J. Magn. Soc. Jpn.*, **38**, 79-82(2014)

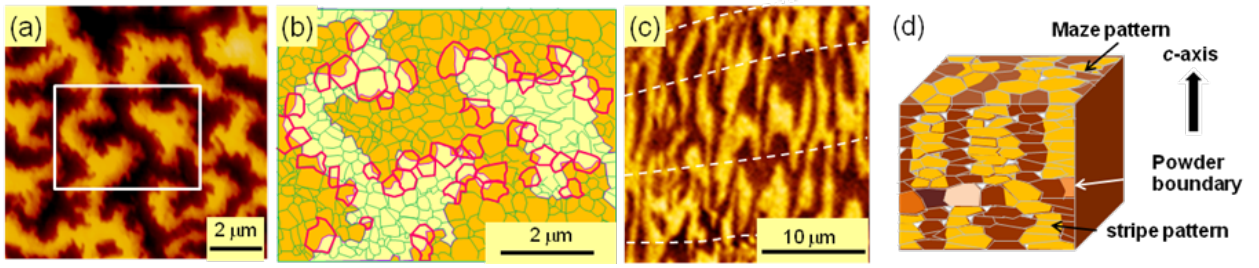

Fig. 1.　(a)(c) MFM images in the thermally demagnetized state. Looking at the planes (a) perpendicular and (c) parallel to the c-axis, respectively. Dotted lines indicate powder boundaries. (b) Illustration of magnetic domain pattern shown in Fig. 1(a) in the white square. Contours of grains observed using LV-SEM are overlaid. Multi-domain grains are shown in bold lines. (d) Illustrations of three dimensional magnetic domain structure of hot-deformed magnet in the thermally demagnetized state.

Observation of magnetic domain reversals in Nd-Fe-B hot-deformed and infiltrated magnets by SANS

M. Yano[1], T. Ueno[2], K. Saito[3], K. Ono[3], M. Harada[4], A. Manabe[1], T. Shoji[1], N. Sakuma[1], A. Kato[1], and U. Keiderling[5]

[1] Advanced Material Engineering Div., Toyota Motor Corporation, Susono 410-1193, Japan
[2]Elements Strategy Initiative Center for Magnetic Materials, National Institute for Materials Science, Tsukuba 305-0047, Japan
[3] High Energy Accelerator Research Organization (KEK), Tsukuba 305-0801, Japan
[4] Toyota Central R&D Labs. Inc., Nagakute 480-1192, Japan
[5]Helmholtz-Zentrum Berlin für Materialien and Energie, Berlin 14109, Germany

Nd-Fe-B magnet in motors in hybrid or electric vehicles requires Dy to increase its coercivity to maintain their magnetization in an operating temperature. However, Dy reduces magnetization in the magnet due to anti-parallel coupling of the magnetic moment between Dy and Fe [1]. To understand the coercivity mechanism in the Nd-Fe-B magnet to satisfy both high coercivity and magnetization, we have studied microstructures and magnetic domains in the magnet.

In general, the coercivity of Nd-Fe-B magnets can be enhanced by reducing the grain size of $Nd_2Fe_{14}B$ phase but it was found that only the grain size reduction cannot realize enough coercivity because of the reversal domain connections during demagnetizing procedures [2]. To reveal factors for higher coercivity, it is important to show the relation among magnetic properties, microstructures and magnetic domain reversals by using several kinds of methods because the microstructures and the magnetic domains are correlated to the coercivity.

Small-angle neutron scattering (SANS) is one of the complementary method to two-dimensional observations using microscope and it has a possibility to quantify the three-dimensional and multi-scaled microstructures and magnetic domains. The SANS enables us to investigate the bulk magnets using high transmission neutrons. Moreover, SANS can be performed under various sample environments of magnetic fields or temperatures.

In order to clarify the effect of grain isolation in nano-crystalline Nd-Fe-B magnets, we have prepared samples with different grain isolation and have performed SANS measurement to observe the difference in microstructures and magnetic domain reversals in these samples.

The hot-deformed Nd-Fe-B magnets have been made from rapidly quenched melt-spun ribbons. The melt-spun ribbons were crushed into a few hundred μm and then sintered at 873 K under a pressure of 100 MPa. The sintered bulk was hot-deformed with height reduction of about 80% to develop a (001) texture of phase. The hot-deformed magnet was soaked into the molten Re-Cu (Re=Pr or Nd) alloys to infiltrate into the grain boundaries to isolate grains [3]. The magnetic properties of as-deformed and Pr-Cu infiltrated samples are shown in Fig. 1 (a).

The SANS was performed at the V4 beamline of the research reactor BER-II at Helmholtz-Zentrum Berlin (HZB), Germany. The samples were fully magnetized along the easy magnetization axis ([001]-axis) at 10 T in advance. The sample temperature was set to 300 K. Neutron beam with the wavelength of 1.147 nm was used. Incoming beam direction was perpendicular to the [001]-axis and the irradiated area at the sample was set to 8 mm in diameter by the neutron window. The typical q range was 0.013–0.165 nm^{-1} with a sample-detector distance of 15.76 m. External magnetic fields of ± 5 T were applied along the [001]-axis to obtain magnetic field-dependent SANS patterns.

The magnetic field dependences of intensity I(q) along the [001]-perpendicular direction for as-deformed and Pr-Cu infiltrated samples are shown in Fig. 1 (b). Note that the scattering vector q and the dimension in real space d can be converted using Bragg equation, $d = 2\pi/q$. The variation of the intensities in a specific q-range corresponds to the variation of the microstructure or magnetic domains of the dimension d. As shown in Fig. 1 (b), the intensities increase by applying the reversal field for as-deformed sample and become maximum at the coercive field of $\mu_0 H_c = -1.46$ T. For

the infiltrated sample, intensities along the [001]-perpendicular direction also increase by applying the reversal field, as observed in the as-deformed sample, but the intensity difference is smaller. To magnify the magnetic field dependence as a function of the q or d, the intensity difference from that at 5 T are shown in Fig. 1 (c). The intensity difference becomes maximum at the coercive field of each sample. The intensity of smaller d range is dominant for as-deformed sample although the intensity of larger d range is dominant for infiltrated sample. These results indicate that the single particle reversal is dominant in the infiltrated sample implying that the larger ratio of the isolated grains than that of the interacting grains in the [001]-perpendicular direction, as compared to the as-deformed one.

These SANS results will be compared with the results of Nd-Cu infiltrated samples or direct magnetic domain observation by microscope.

Reference

[1] J. F. Herbst and W. B. Yelon, J. Appl. Phys. **57**, 2343 (1985).

[2] M. Yano *et al*., IEEE Trans. Mag., **48**, 2804 (2012).

[3] H. Sepehri-Amin *et al*., Acta Materia., **61**, 6622 (2013).

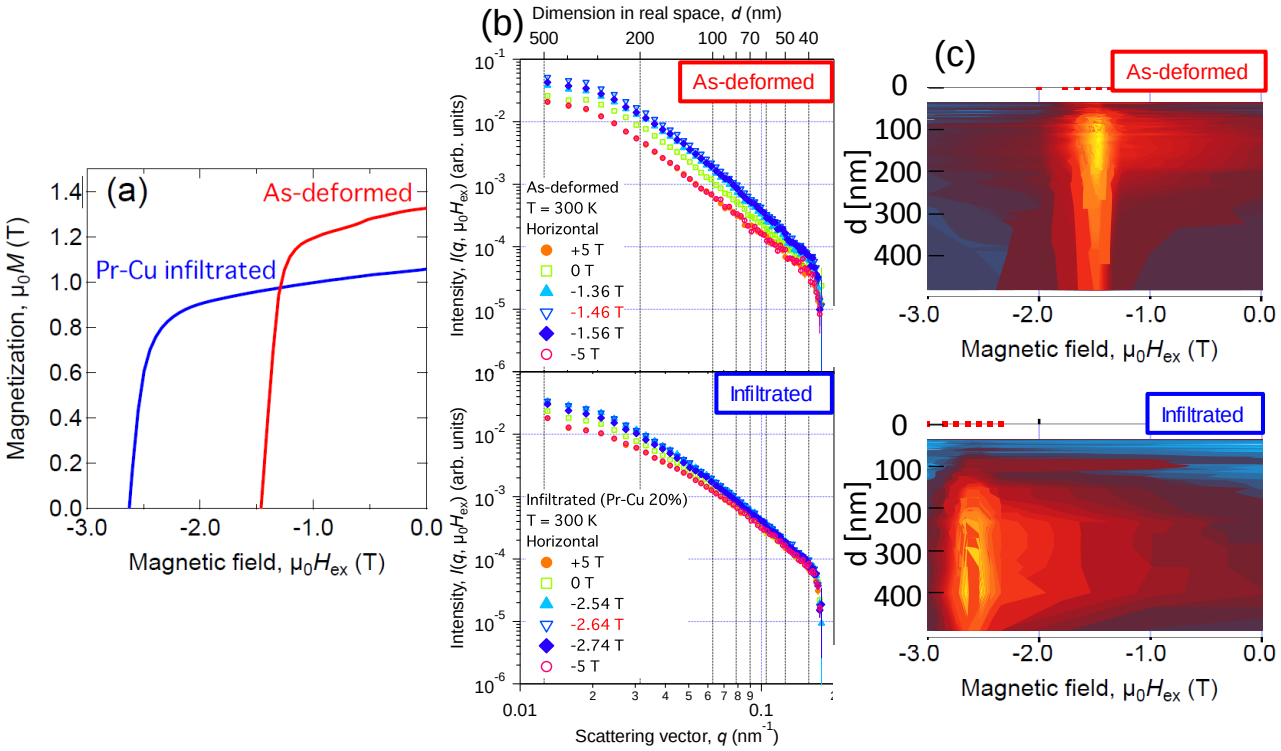

Fig. 1 (a) Demagnetization curves for as-deformed and Pr-Cu infiltrated Nd-Fe-B nano-crystalline magnets. (b) Magnetic field dependence of SANS intensities of as-deformed and infiltrated magnets. (c) Intensity difference between fully magnetized state and each demagnetization field. These intensity maps can be produced by (b).

Large-Scale Micromagnetic Simulation of Reversal Processes in Nd-Fe-B Magnets

A. Furuya[1], J. Fujisaki[1], K. Shimizu[1], T. Tanaka[1], T. Ataka[1], Y. Uehara[1], H. Oshima[2], T. Ohkubo[3], S. Hirosawa[3] and K. Hono[3]
[1]Fujitsu Limited, Kawasaki 211-8588, Japan
[2]Fujitsu Laboratories Limited, Atsugi 243-0197, Japan
[3]National Institute for Materials Science, Tsukuba 305-0047, Japan

Introduction:

Nd-Fe-B sintered magnets which have high maximum energy product and coercivity are widely used in electric motors and generators. To improve their properties, theoretical elucidation of the reversal process is demanded. In particular, the relationship between coercivity and their microscopic structures is an important topic for the improvement both from the scientific and technological points of view [1, 2]. To understand coercivity mechanism, theoretical studies based on micromagnetics have been performed to analyze the reversal process in Nd-Fe-B magnets. However, the edge length of numerical mesh element has to be smaller than the exchange length (1.7nm in Nd-Fe-B phase) in order to avoid “artificial pinning” in the simulation. Typically, grain size of sintered Nd-Fe-B magnets is from 100nm to 10μm. To simulate the pinning and nucleation process in the realistic grain structures, therefore, the number of finite elements involved in the numerical calculations exceeds a huge value of the order of millions. In this study, large-scale micromagnetic simulation is performed on K computer [3]. The effects of microstructure on the coercivity are numerically investigated.

Calculation methods:

We consider the following micromagnetic energy E_{tot} to analyze the magnetization in the simplified microstructure of Nd-Fe-B magnets,

$$E_{tot} = E_{Zeeman} + E_{exc} + E_{ani} + E_d , \tag{1}$$

where, E_{Zeeman}, E_{exc} , E_{ani} and E_d are Zeeman energy, exchange energy, anisotropy energy and magneto-static energy, respectively. The magnetization dynamics of the reversal processes are simulated by calculating the Landau-Lifshitz-Gilbert (LLG) equation,

$$(1+\alpha^2)\frac{\partial \boldsymbol{m}}{\partial t} = -\gamma\left(\boldsymbol{m}\times\boldsymbol{H}_{eff}\right) - \gamma\alpha\boldsymbol{m}\times\left(\boldsymbol{m}\times\boldsymbol{H}_{eff}\right), \tag{2}$$

where, m, γ and α are the normalized magnetization vector, the gyro-magnetic ratio, and the Gilbert damping factor. The effective field $\boldsymbol{H}_{eff}$ is derived from partial derivative of magnetization energies. The spatial distribution of the magnetization vector is numerically divided to the elements of the unstructured mesh which is commonly used in finite element method. To handle the domain wall motion and nucleation of the reverse domains, we used a small mesh size(1nm) and adapted the domain decomposition method by using METIS library, which divided the entire model in the small region and each region was calculated by the separate CPUs [4].

Simulations:

The simulation model is shown in Fig.1. This model is composed of 27 grains whose diameter is 50 nm. The grains are three-dimensionally aligned and the width of grain boundary is 2 nm. The total number of mesh model is about 5 million. We here label the state of a magnetic vector which points to positive y-direction “up”, and the opposite state “down”. As shown in Fig.1, all the initial magnetic vectors are down except for those in the grain of the front side of the top layer, which are initially in the up state. The simulated reversal process in the case of the alignment α=1 is shown in Fig.2. Due to the inclusion of the soft magnetic layers in the grain boundaries, the reversal domain easily propagates into neighboring grains. The simulation result at the alignment α=0.5 is also shown in Fig.3.

This result shows that the grain boundaries pin the domain wall of initial reverse domain and the nucleation occurs at another grains. The reversal mechanism depends on the microstructure and material parameters of the grain boundaries. In the presentation, the parameter dependences of the reversal processes and coercivity will be reported in detail.

Acknowledgment

This research used computational resources of the K computer provided by the RIKEN Advanced Institute for Computational Science through the HPCI System Research project (Project ID: hp120086).

References

1) Y. Matsuura; Proc. of the 22nd REPM (2012) pp.147-150
2) H. Sepehri-Amin, T. Ohkubo, T. Shima, and K. Hono, Acta Mater. 60, 819 (2012).
3) http://www.aics.riken.jp/en/kconmuputer/ ,Homepage of RIKEN Advanced Institute for Computatonal Science
4) G. Karypis and V. Kumar. SIAM Journal on Scientific Computing, 20 (1999) 359

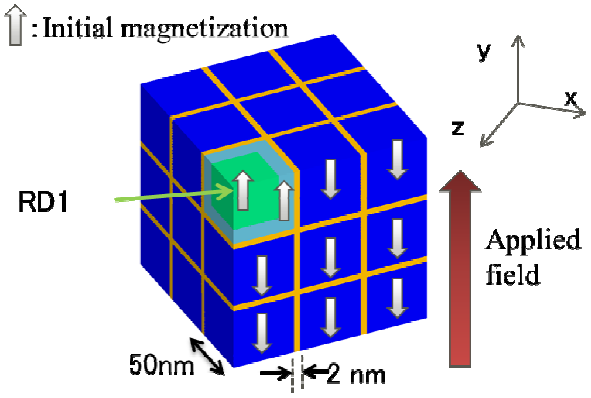

Fig. 1 Simulation Model of multi-grain structure

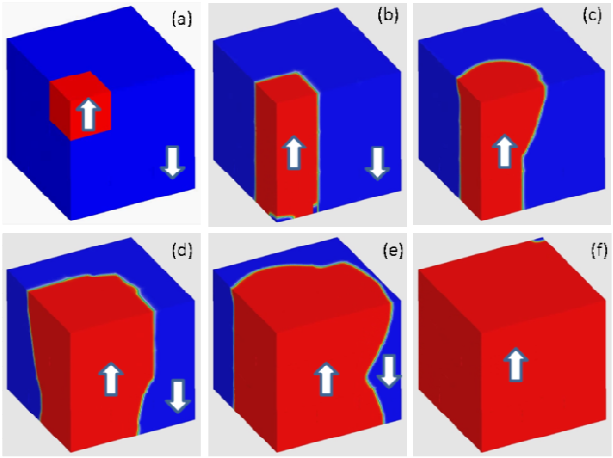

Fig. 2 Contour plot of m_z in the case of alignment parameter α=1.

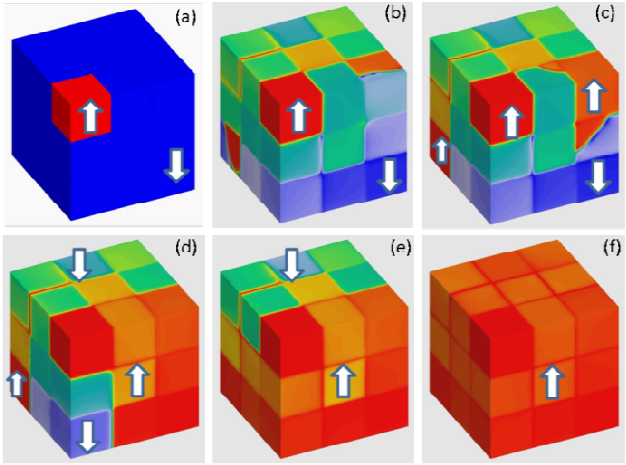

Fig. 3 Contour plot of m_z in the case of alignment parameter α=0.5

Anisotropy inducement mechanism in hydrogen disproportionation desorption recombination (HDDR) processed Nd-Fe-B powders

H. Sepehri-Amin[1], T. Ohkubo[1], K. Hono[1], K. Güth[2], and O. Gutfleisch[2,3]

[1]Elements Strategy Initiative Center for Magnetic Materials, NIMS, Tsukuba, Japan
[2]Fraunhofer ISC Projektgruppe IWKS, Germany
[3]Materialwissenschaft, Technische Universität Darmstadt, Germany

Introduction

The hydrogenation-disproportionation-desorption-recombination (HDDR) process is an attractive and unique method for producing anisotropic nanocrystalline Nd-Fe-B powders. In order to develop highly textured Nd-Fe-B powders, HDDR process parameters need to be carefully chosen and controlled [1]. Although lots of investigations have been carried out to understand the mechanism of the anisotropy development in HDDR powders [1-3], some questions still remain. In this work, the microstructures of Nd-Fe-B powders that were HD processed at different hydrogen pressure (P_{H2}^{HD}) were investigated to fully clarify the mechanism of the anisotropic microstructure evolution.

Experimental

Dynamic hydrogenation disproportionation (HD) desorption recombination (DR) process was carried out on $Nd_{12.8}Fe_{80.1}B_{6.6}Ga_{0.3}Nb_{0.2}$ alloy powders at different HD hydrogen pressure, P_{H2}^{HD} = 30 kPa and 100 kPa. The microstructures of the samples in early stages of the HD process, a fully HD process, and an early DR process were investigated using SEM/FIB (Carl Zeiss 1540EsB), TEM (Titan G2 80-200), and a locally built laser-assisted three dimensional atom probe (3DAP) to characterize the memory sites responsible for the texture development.

Results

A high remanent magnetization of 1.43 T was obtained for the fully HDDR processed powder with P_{H2}^{HD} = 30 kPa, indicating a strong [001] crystallographic texture. However, P_{H2}^{HD} = 100 kPa led to weakly textured Nd-Fe-B powders with a remanent magnetization of 0.89 T.

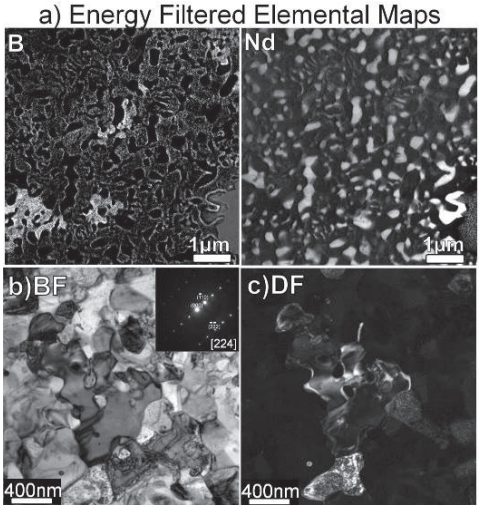

Fig. 1: (a) Energy filtered B and Nd maps of fully HD processed sample at P_{H2}=30kPa. (b) BF and (c) DF TEM images from the same sample indicating well textured Fe_2B grains. SADP obtained from a Fe_2B grain is shown in inset of (b).

TEM observations from early HD processed powder with P_{H2}^{HD} = 30 kPa showed that the Fe_2B phase has a direct crystallographic orientation relationship with the initial $Nd_2Fe_{14}B$ grains, i.e. $[420]_{Fe2B}||[211]_{Nd2Fe14B}$ and $(00\bar{2})_{Fe2B}||(\bar{1}\,11)_{Nd2Fe14B}$. Energy filtered (EF)-TEM and 3DAP results obtained from a fully HD processed sample showed boron not only in the Fe_2B phase but also at the NdH_2/α-Fe interfaces in both weakly and highly textured samples. High resolution STEM-HAADF image and nano-beam diffraction analysis from NdH_2/α-Fe interfaces showed that boron enrichment at these interfaces does not make a separate phase, such as iron boride. However, there is boron enrichment more in Fe grain of the NdH_2/α-Fe interface in nano-scale. Fig. 1(a) shows EF-TEM maps of B and Nd for the fully HD processed sample with P_{H2}^{HD} = 30 kPa. Bright field (BF)-TEM images obtained from the fully HD processed samples with different P_{H2}^{HD} showed that the Fe_2B regions in both

weakly and highly textured samples comprise of several small Fe_2B grains. Fig. 1 (b) and (c) shows BF and dark field (DF)-TEM images obtained from fully HD processed P_{H2}^{HD}=30 kPa sample. The DF-TEM image shows that the Fe_2B sub-grains in boride region of fully HD processed P_{H2}^{HD} = 30 kPa sample is strongly textured. Fig. 2 (a) shows BF-TEM image taken from the sample fully HD processed at P_{H2}^{HD} = 100 kPa. Superimposed EF-TEM maps of Nd (red), Fe (Blue), and B (green), obtained from the same region as Fig. 2(a), is shown in Fig. 2 (b). By comparing Fig. 2 (a) and (b), NdH_2, α-Fe, and Fe_2B phases can be distinguished. Selected area diffraction patterns obtained from different Fe_2B grains in boride area are shown in Fig. 2(c), indicating that the Fe_2B grains in the boride area are not well aligned in the sample fully HD processed at P_{H2}^{HD} = 100 kPa. Orientation relationship study of P_{H2}^{HD} = 30 kPa sample at early DR processed stage showed that recombined $Nd_2Fe_{14}B$ grains have direct orientation relationship with the remaining Fe_2B phase from HD process. In addition, 3D SEM tomography obtained from 3D serial sectioning of BSE images from P_{H2}^{HD} = 30 kPa sample at very early stage of DR process showed that the recombined $Nd_2Fe_{14}B$ grains nucleate at the interface of Fe_2B/NdH_2 grains and grow through the interface of NdH_2/α-Fe grains.

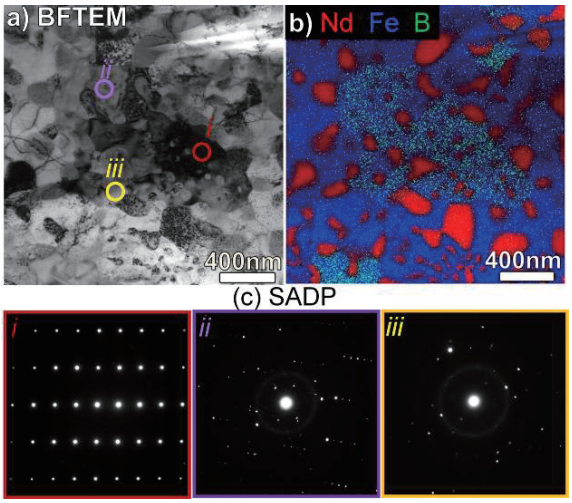

Fig. 2: (a) Bright field TEM image and (b) superimposed energy filtered Nd, Fe, and B maps of fully HD processed sample at P_{H2}=100kPa. (c) Selected area diffraction patterns obtained from different Fe_2B sub-grains in boride region.

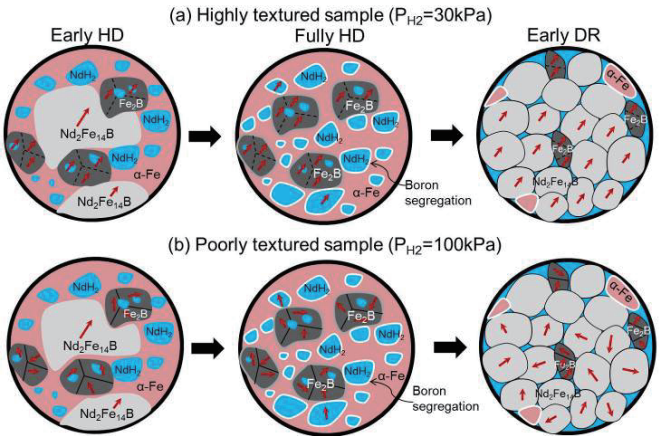

Fig. 3: Schematic illustration of microstructure evolution of HDDR processed sample with (a) P_{H2}^{HD} = 30 kPa (b) P_{H2}^{HD} = 100 kPa. This figure shows that in the highly textured powder, highly aligned Fe_2B grains act as memory sites and remembering the crystallographic orientation of initial $Nd_2Fe_{14}B$ grains and transferring the same orientation to the recombined $Nd_2Fe_{14}B$ grains.

These microstructure investigations indicate that the highly aligned Fe_2B grains act as memory sites for the development of the texture in the sample HD processed at P_{H2}^{HD} = 30 kPa, as shown schematically in Fig. 3, consistent with the previously proposed texture memory effect (TME) model. Importantly, it can now be shown that the recombined $Nd_2Fe_{14}B$ phase nucleates at the interface of Fe_2B with NdH_2 phase and grow through the interface of NdH_2/α-Fe interfaces and boron segregated at the NdH_2/α-Fe interface acts as a boron source for the growth of the recombined $Nd_2Fe_{14}B$ grains during DR process.

Reference

[1] O. Gutfleisch et al. IEEE Trans. Magn. 39 (2003) 2926.
[2] T. Tomida et al. Acta Mater. 47 (1999) 875.
[3] Y. Honkura et al. JMMM 290-291 (2005) 1282.